

Article

Collective Magnetic Behavior of 11 nm Photo-Switchable CsCoFe Prussian Blue Analogue Nanocrystals: Effect of Dilution and Light Intensity

 Linh Trinh, Eric Rivière , Sandra Mazerat, Laure Catala and Talal Mallah * 

Institut de Chimie Moléculaire et des Matériaux d'Orsay, Université Paris-Saclay, CNRS 15, Rue Georges Clémenceau, CEDEX 09, 91405 Orsay, France; trinh.linh@universite-paris-saclay.fr (L.T.); eric.riviere@universite-paris-saclay.fr (E.R.); sandra.mazerat@universite-paris-saclay.fr (S.M.); laure.catala@universite-paris-saclay.fr (L.C.)

* Correspondence: talal.mallah@universite-paris-saclay.fr

Abstract: The collective magnetic behavior of photoswitchable 11 nm cyanide-bridged nanoparticles based of the Prussian blue analogue CsCoFe were investigated when embedded in two different matrices with different concentrations. The effect of the intensity of light irradiation was studied in the less concentrated sample. Magnetization studies and alternating magnetic susceptibility data are consistent with a collective magnetic behavior due to interparticle dipolar magnetic interaction for the two compounds, even though the objects have a size that place them in the superparamagnetic regime.

Keywords: Prussian blue analogue; photomagnetism; nanocrystals; photo-switchable; magnetic properties; dipolar interaction



Citation: Trinh, L.; Rivière, E.; Mazerat, S.; Catala, L.; Mallah, T. Collective Magnetic Behavior of 11 nm Photo-Switchable CsCoFe Prussian Blue Analogue Nanocrystals: Effect of Dilution and Light Intensity. *Magnetochemistry* **2021**, *7*, 99. <https://doi.org/10.3390/magnetochemistry7070099>

Academic Editors: Carlos J. Gómez García, John Wallis, Lee Martin, Scott Turner and Hiroki Akutsu

Received: 7 May 2021
Accepted: 6 July 2021
Published: 8 July 2021

Publisher's Note: MDPI stays neutral with regard to jurisdictional claims in published maps and institutional affiliations.



Copyright: © 2021 by the authors. Licensee MDPI, Basel, Switzerland. This article is an open access article distributed under the terms and conditions of the Creative Commons Attribution (CC BY) license (<https://creativecommons.org/licenses/by/4.0/>).

1. Introduction

Prussian blue analogues are cyanide-bridged coordination networks with a face centered cubic (fcc) structure and general formula $A_y\{M[M'(CN)_6]_{1-x}\square_x\} \cdot zH_2O$, where A is an alkali metal ion (Na, Rb or Cs in most cases), M and M' are transition metal ions of the first series with in most cases oxidation states II and III, respectively, and \square stands for metalocyanide vacancies. The cell parameter is close to 10 Å and corresponds to the distance between two metal ions of the same nature. Water molecules occupy the tetrahedral sites of the fcc structure and can also be coordinated to M when vacancies are present. When $M' = Fe$ and $M = Co$, the two states $Co^{II}Fe^{III}$ ($S_{Co^{II}} = 3/2$, $S_{Fe^{III}} = 1/2$) and $Co^{III}Fe^{II}$ ($S_{Co^{III}} = 0$, $S_{Fe^{II}} = 0$) are close in energy and it is possible to switch from one to another thermally or by light irradiation at low temperatures. The electron transfer is accompanied by a spin crossover on Co (from high spin Co^{II} ($S_{Co^{II}} = 3/2$) to low spin Co^{III} ($S_{Co^{III}} = 0$)), inducing a large change in the magnetic response as first demonstrated by Hashimoto [1]. More precisely, depending on the nature of the alkali metal ions that occupy the tetrahedral sites or its absence and on the vacancies concentration, three situations may be encountered: (i) the magnetic state $Co^{II}Fe^{III}$ is present at high temperature and no electron transfer occurs upon cooling (this is the case in the absence or for low contents of alkali ions); (ii) the diamagnetic state $Co^{III}Fe^{II}$ is present for the whole temperature range, but no light induced electron transfer occurs at low temperature (this is the case when Cs^+ occupy the tetrahedral sites. For this case, the compound contains generally some amount of the $Co^{II}Fe^{III}$ magnetic phase); and (iii) the magnetic state is present at high temperature and upon cooling down a thermally assisted electron transfer occurs leading to the diamagnetic state $Co^{III}Fe^{II}$ that may be transformed upon light irradiation to $Co^{II}Fe^{III}$ at low temperature (this occurs usually when $A = Rb$ or when the concentration of Cs is well below 1 (see formulae above)). These different cases were thoroughly investigated and rationalized for the bulk materials [2–7], made of aggregates of nanoparticles in the hundred nanometers size range.

Recently we reported [8], the photoswitching behavior of nanocrystals in the sub-15 nm size containing a large concentration of Cs and almost no vacancies i.e., $(\text{CTA})_{0.4}[\text{Cs}_{0.7}\text{Co}\{\text{Fe}(\text{CN})_6\}_{0.9}]\bullet\text{H}_2\text{O}$ that have a majority of the diamagnetic phase at room temperature and present a light induced switching to the magnetic state at low temperatures. The photoswitching behavior was studied when the particles were embedded in Cetyltrimethylammonium (CTA^+) which serves as counter-cation for the nanocrystals and for the objects surrounded by the organic polymer polyvinylpyrrolidone (PVP). However, we did not report the collective magnetic behavior of the nanocrystals in the photo-induced state. Indeed, upon irradiation the diamagnetic ions become paramagnetic and, due to an antiferromagnetic exchange coupling interaction, a collective ferrimagnetic behavior is observed in the bulk with a critical temperature close to 20 K [1]. In nanoparticles, the situation may be different since the magnetic correlation length is limited by the particles' size if the interparticle magnetic coupling is absent. The nanocrystals we reported are stabilized as colloids in water in the absence of stabilizing agents so that they can be embedded in different matrices and with different concentrations [9]. The objective of this paper is to investigate the effect of dilution and intensity of light irradiation on the magnetic behavior of the nanocrystals in the photoinduced metastable state when embedded in CTA and PVP.

2. Results and Discussion

2.1. Materials and Methods

The preparation and full characterization of the nanocrystals were recently reported [8]. The nanocrystals were prepared in water as a stable colloidal solution then recovered by CTA^+ and by PVP to give two samples, namely CsCoFe_CTA and CsCoFe_PVP . The two materials were prepared as follows.

CsCoFe_CTA. 200 mL of distilled water containing 673 mg of CsCl (4 mM) and 476 mg (2 mM) of $[\text{Co}(\text{H}_2\text{O})_6]\text{Cl}_2$ were quickly added to 200 mL of distilled water containing 658 mg (2 mM) of $\text{K}_3[\text{Fe}(\text{CN})_6]$. The solution was vigorously mixed for 30 min. A methanolic solution (600 mL) containing 1.10 g (6 mM) of cetyltrimethylammonium bromide (CTABr) was added dropwise to 200 mL (half) of the aqueous solution containing the nanoparticles. A precipitate formed during the addition, and it was recovered by centrifugation (9000 rpm for 20 min) washed with a small amount of water and dried under vacuum overnight. Elemental analysis for $\text{Cs}_{0.7}(\text{C}_{19}\text{H}_{42}\text{N})_{0.4}\text{Co}[\text{Fe}(\text{CN})_6]_{0.9}(\text{H}_2\text{O})$, exp. (calc.) C: 20.10 (20.60), H: 2.43 (3.79), N: 17.70 (17.12).

CsCoFe_PVP. The remaining 200 mL of the colloidal solution containing the nanoparticles was added dropwise for 3 h to 20 mL of an aqueous solution containing 12 g of PVP. Then, 900 mL of acetone is added. A precipitate formed, and it was recovered by centrifugation (9000 rpm for 20 min), washed with a small amount of acetone, and dried under vacuum overnight.

A Transmission Electron Microscopy (Jeol 1400, Jeol, Tokyo, Japan) image of the CTA materials showed objects with an average size close to 11 nm (Figure 1). The X-ray power diffraction (Panalytical X-Pert Pro MPD, Malvern Panalytical, Malvern, UK) diagram of the same material was consistent with face centered cubic structure as expected for Prussian blue analogues with a cell parameter $a = 10.01 \text{ \AA}$ (Figure 1) [8]. The infrared spectrum (Perkin Elmer Spectrum 100, PerkinElmer Inc., Norwalk, Connecticut, USA) (Figure 1) in the $2300\text{--}1900 \text{ cm}^{-1}$ regions showed the asymmetric vibration mode of the cyanide at 2115 cm^{-1} characteristics of cyanide bridge corresponding to a mixture of Fe(II)-CN-Co(III) and Fe(II)-CN-Co(III) sequences [8].

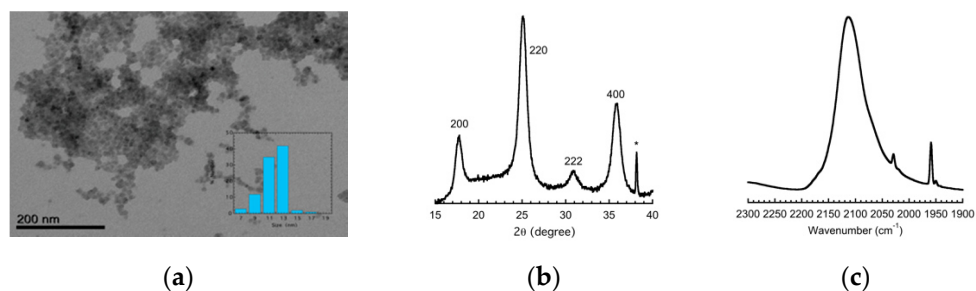


Figure 1. (a) Transmission Electron Microscopy imaging with count as a function of size in the inset; (b) Powder X-ray diffraction pattern; and (c) infra-red spectrum of the CsCoFe_CTA nanoparticles.

Combined powder X-ray diffraction, magnetic, Electron Paramagnetic Resonance, and X-ray photoelectron spectroscopy studies are consistent with the presence at room temperature of the different phases $\text{Co}^{\text{II}}\text{Fe}^{\text{II}}$, $\text{Co}^{\text{II}}\text{Fe}^{\text{III}}$, and $\text{Co}^{\text{III}}\text{Fe}^{\text{II}}$, the latter contributing to 70% of the overall concentration of each nanocrystal [8]. Because of their stability as isolated objects in water, they were used to unravel the mechanisms of charge transfer and spin crossover after light irradiation [10]. They were also deposited on graphite and their conductance was measured, showing a long range electron transport with relatively weak attenuation [11].

In order to assess the relative concentration in nanoparticles for the two materials, we compared their magnetization (Quantum Design XL7, Quantum Design, San Diego, CA, USA) values at saturation (M_{sat}) and at low temperature ($T = 2 \text{ K}$ and $B = 6 \text{ T}$) that are proportional to the amount magnetic species within the material (Figure 2). A ratio close to 20 was found for $M_{\text{sat}(\text{CTA})}/M_{\text{sat}(\text{PVP})}$, showing that the concentration in nanoparticles of the PVP containing materials was 20 times lower than that of the CTA one.

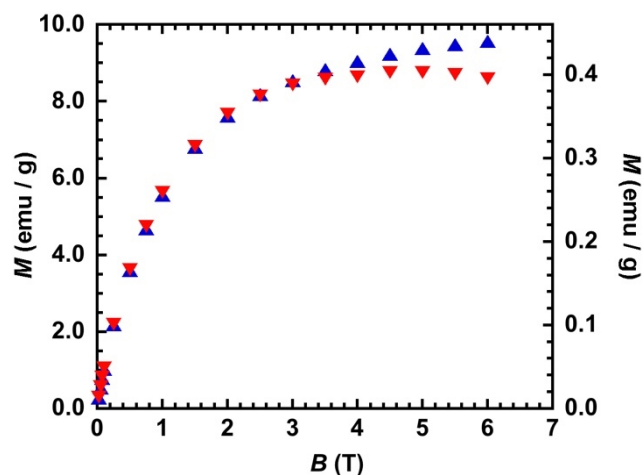


Figure 2. $M = f(B)$ at $T = 2 \text{ K}$ before irradiation for CsCoFe_CTA and CsCoFe_PVP. ▲: left scale; ▼: right scale.

The magnetic behavior of the two samples CsCoFe_CTA and CsCoFe_PVP was studied using a SQUID magnetometer in the dc mode by measuring the magnetization in the Field Cooled (FCM) and the Zero-Field Cooled (ZFCM) modes and the magnetic hysteresis loops at $T = 2 \text{ K}$ and in the ac mode by measuring the thermal dependence of the in-phase and out-of-phase magnetic susceptibilities in zero dc applied magnetic field for different frequencies of the alternating magnetic field equal to 3 Oe. The irradiation was carried out using a laser diode connected to an optical fiber at a wavelength of 635 nm with the values of the laser power specified below.

2.2. Magnetic Behavior of CsCoFe_CTA

Before irradiation, the FCM plot has the feature of paramagnetic species with only a slight increase below $T = 4$ K, consistent with the presence of the paramagnetic species $\text{Co}^{\text{II}}\text{Fe}^{\text{II}}$ and $\text{Co}^{\text{II}}\text{Fe}^{\text{III}}$ (Figure 3a). It is worth noting that the absence of a large increase of the magnetization at low temperature is in line with a very short correlation length consistent with relatively isolated $\text{Co}^{\text{II}}\text{Fe}^{\text{III}}$ pairs within the nanocrystals. The sample was irradiated at $T = 2$ K, heated up to 25 K, and the FCM was measured. After irradiation, the shape of the FCM curve suggests a behavior due to a magnetic order or to a blocking of the magnetization. The ZFCM curve after irradiation shows a maximum at $T = 11.8$ K and meets the FCM curve at $T = 14.5$ K, which is usually associated with the blocking of particles with different sizes.

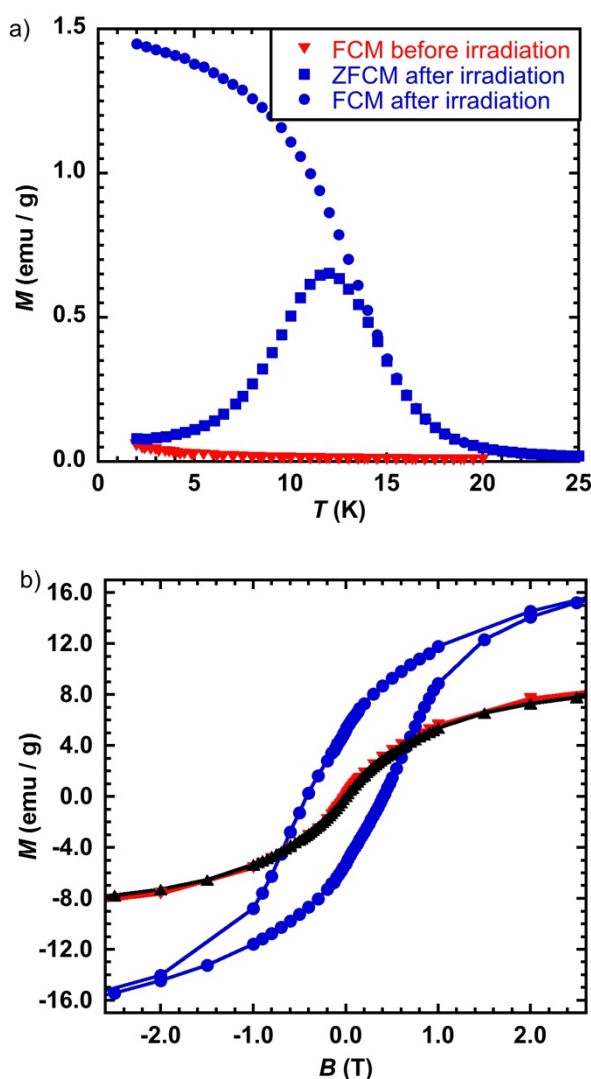


Figure 3. (a) $M = f(T)$ in the form of Field Cooled before (\blacktriangledown) and after (\bullet) irradiation and Zero-Field Cooled after irradiation (\blacksquare) and (b) Magnetic hysteresis loop at $T = 2$ K before (\blacktriangledown) and after (\bullet) irradiation and after relaxation (\blacktriangle), for CsCoFe_CTA; laser power = 50 mW/cm².

The magnetic hysteresis loop measured before irradiation was characteristic of a paramagnetic behavior (Figure 3b), without an opening at zero field. After irradiation, a hysteresis loop appeared with a coercive field $H_C = 0.41$ T, consistent with a relatively large magnetic anisotropy for the photoinduced state as expected from the presence of Co^{II} within the nanoparticles [12]. In order to check the reversibility of the photoswitching, the sample was heated to $T = 250$ K (above its relaxation temperature) [8] and then cooled

down to 2 K. The magnetization after relaxation was superimposable to its trace before irradiation, confirming the total recovery of the ground state.

We performed ac susceptibility studies in order to get more insight into the magnetism of the system. Before irradiation, there was no maxima in the temperature dependence of the in-phase (χ') susceptibility responses for frequencies (ν) ranging from 0.1 to 300 Hz (ac magnetic field of 3 Oe and zero dc magnetic field). After irradiation, maxima of the $\chi' = f(T)$ and the $\chi'' = f(T)$ (χ'' is the out-of-phase susceptibility) curves appeared (Figure 4), which are typical for a system with a blocking temperature that can be associated with the isolated objects or due to a spin glass like behavior. The value of the maximum of the $\chi'' = f(T)$ curve at the lowest frequency available ($\nu = 0.1$ Hz) was 11.2 K, consistent with temperature of the maximum of the ZFCM curve. The analysis of the out-of-phase data was performed by plotting the $\ln(\tau) = f(1/T)$ (with $\tau(1/2\pi\nu) = \tau_0 \exp(\Delta E/kT)$, where τ_0 is the attempt time, ΔE the anisotropy barrier, k the Boltzmann constant, and T the temperature of the maximum of the $\chi'' = f(T)$ curve at a given frequency. The linear fit of the data (not shown) led to $\tau_0 = 1.2 \times 10^{-27}$ s and $\Delta E = 690$ K. For single magnetic domain nanoparticles without (or with very weak) dipolar interactions, values for τ_0 close or larger than 10^{-12} s were expected [13], and were found for isolated CsNiCr cyanide-bridged nanoparticles [14]. The τ_0 value obtained from the fit had no physical meaning for isolated objects and it can be assumed that the observed behavior was due to magnetic interactions among the particles. The Mydosh parameter ϕ allows for discriminating among various magnetic behaviors where $\phi = (T_{\max} - T_{\min}) / (T_{\max}(\log \nu_{\max} - \log \nu_{\min}))$ with T_{\max} and T_{\min} being the temperatures of the maxima of the $\chi'' = f(T)$ curves for the two extreme applied frequencies ν_{\max} and ν_{\min} respectively, ϕ values close or larger than 0.12 are expected for nearly isolated magnetic nanoparticles [13,15]. For the present case, ϕ (0.03) was much smaller than 0.12, which indicates together with the very small τ_0 value the presence of magnetic interactions (dipolar) among the particles and not to a blocking of the magnetization of single domain isolated objects. It is possible to fit the relaxation time by introducing a parameter that accounts for the interaction using the modified Arrhenius law $\tau = \tau_0 \exp(\Delta E/k(T - T_0))$, where T_0 considers the interaction among the nanoparticles that leads to more physically acceptable values for τ_0 (2.2×10^{-12} s) and an average anisotropy barrier $\Delta E = 114$ K with $T_0 = 7$ K.

2.3. Magnetic Behavior of CsCoFe_PVP

Here, the nanocrystals were embedded in PVP with a concentration 20 times less. They are, therefore, spatially more separated than in CsCoFe_CTA.

The maximum of the ZFCM curve was found at $T = 4.4$ K, a value smaller than for CsCoFe_CTA (11.8 K) (Figure 5a). The FCM and ZFCM curves joined at $T = 5$ K. The difference in the temperature between the maximum of the ZFCM and the temperature where the two curves join was 0.6 K, which was lower than 2.7 K found for CsCoFe_CTA. This result means that the difference in the irreversibility temperature and the maximum of the ZFCM curve for CsCoFe_CTA was not due to the blocking of particles with different sizes, otherwise we would have had the same difference for CsCoFe_PVP, since the same objects were present in the two materials. Therefore, magnetic dipolar interactions seem to affect the irreversibility temperature of the magnetization curves in the case of the CsCoFe nanoparticles.

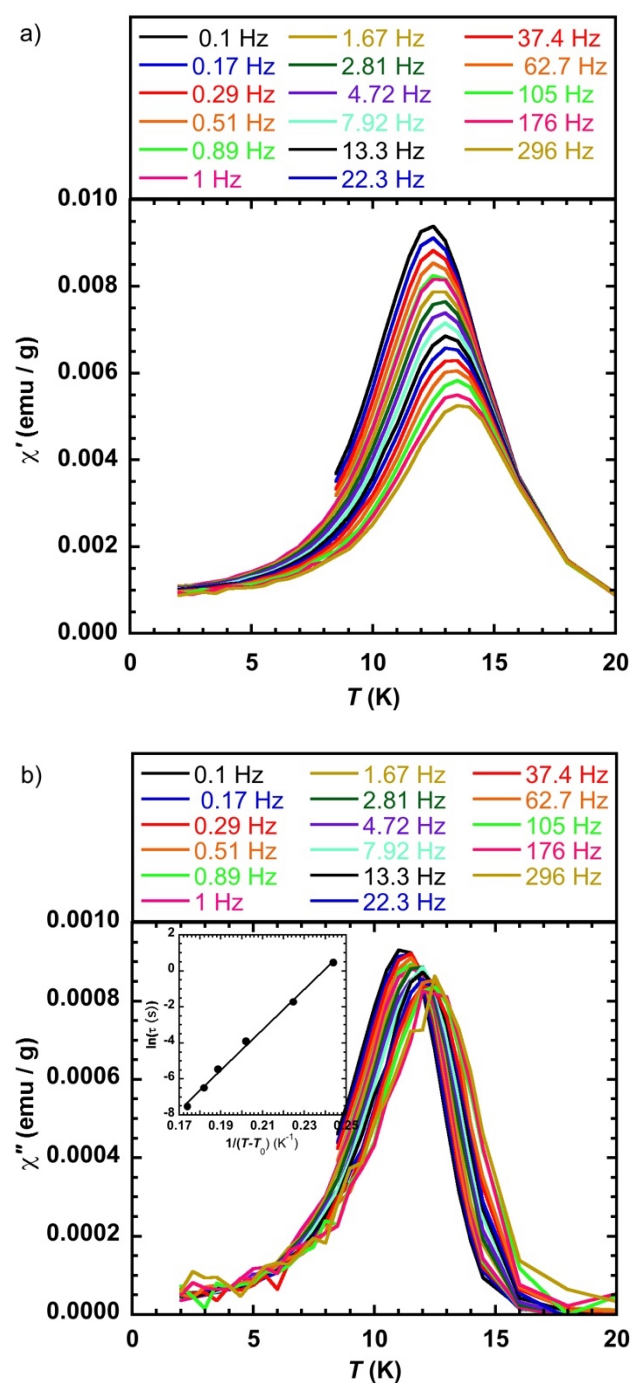


Figure 4. (a) $\chi' = f(T)$ and (b) $\chi'' = f(T)$ at different frequencies of the alternating magnetic field (3 Oe), inset $\ln(\tau) = f(1/(T-T_0))$ and linear fit with values in the text, CsCoFe_CTA; laser power = 50 mW/cm².

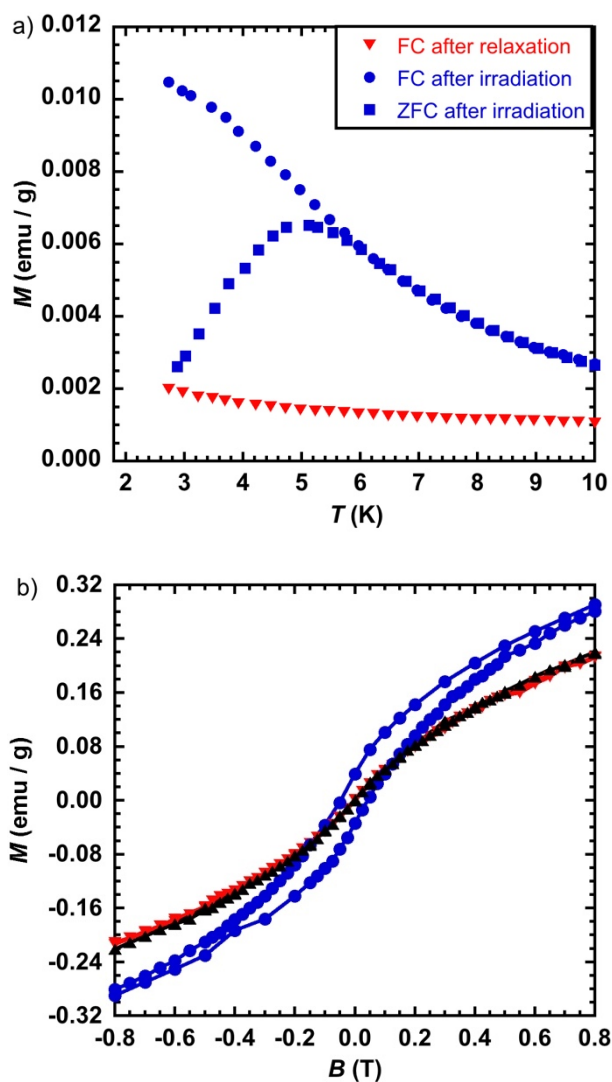


Figure 5. (a) $M = f(T)$ in the form of Field Cooled before (\blacktriangledown) and after (\bullet) irradiation and Zero-Field Cooled after irradiation (\blacksquare), for CsCoFe_PVP and (b) Magnetic hysteresis loop at $T = 2$ K before (\blacktriangledown) and after (\bullet) irradiation and after relaxation (\blacktriangle); laser power 65 mW/cm^2 .

The magnetic hysteresis loop opens after light irradiation with a coercive field of 0.053 T (Figure 5b), one order of magnitude weaker than for the non-diluted CsCoFe_CTA compound. The magnetization curves before irradiation and after relaxation are superimposable, as expected, and are consistent with the reversibility of the process.

The susceptibility measurements with an alternating magnetic field of 3 Oe gave a very weak signal before irradiation, as expected. After irradiation, the light induced data were not of very good quality because we reduced, as much as possible, the thickness of the sample in order to have a maximal light penetration. However, we observed the maxima of the $\chi' = f(T)$ curves at different frequencies that do not coincide (Figure 6a). The temperature dependence of the out-of-phase susceptibility curves measured at 1 and 2.81 Hz shows slightly different temperature maxima (Figure 6b), even though there is some uncertainty concerning these values because of the very weak signal.

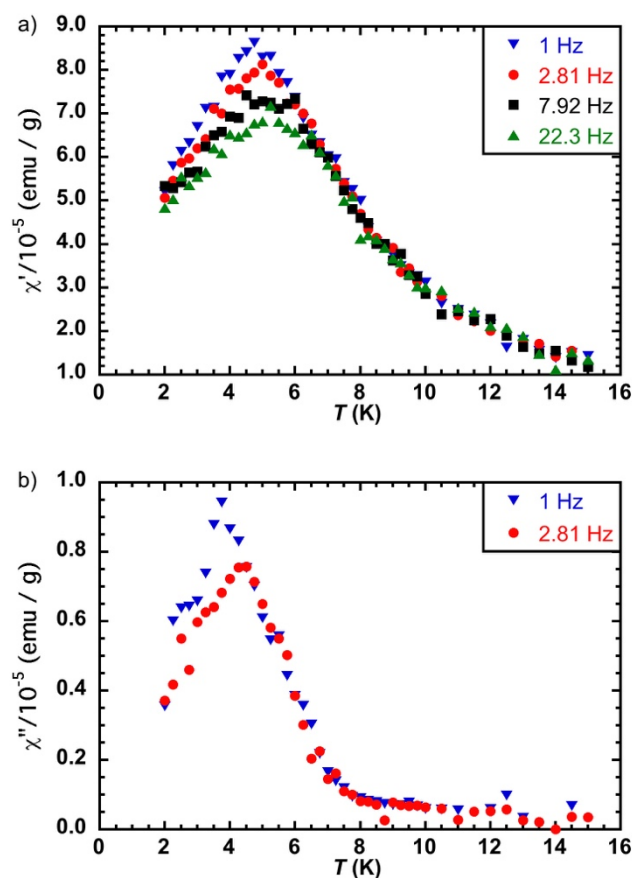


Figure 6. (a) $\chi' = f(T)$ and (b) $\chi'' = f(T)$ at different frequencies of the alternating magnetic field (3 Oe) for CsCoFe_PVP; laser power 65 mW/cm^2 .

A photomagnetic effect leading to an opening of the hysteresis loop was observed as for CsCoFe_CTA, suggesting a similar behavior. However, the maximum of the ZFCM curve is at lower temperature and the out-of-phase susceptibility signals are too low to reach a conclusion of the nature of the magnetic behavior of CsCoFe_PVP. We therefore studied the effect of light intensity on the magnetic behavior of the materials.

2.4. Effect of the Power of Light Irradiation

Another way to sense the effect of magnetic dipolar interactions is to keep the same concentration of the nanoparticles and gradually increase their magnetic moments. Since the magnitude of the magnetic dipolar interactions is proportional to the value of the magnetic moments of the interacting objects, increasing the magnetic moment should lead to an upward shift of the critical temperature (everything else being equal). In order to optimize light penetration and obtain the maximum light-induced response, we used a thin film of few microns of PVP containing the nanoparticles. We first measured the temporal response to light by irradiating the sample at different laser powers at $T = 10 \text{ K}$ and $B = 0.5 \text{ T}$. Figure 7a illustrates the variation of the magnetization (M) with time for a power of 20 mW/cm^2 . It shows that 50% of the saturation is obtained within 8 min and 90% within 30 min. When irradiating at a power of 100 mW/cm^2 (not shown here), 90% of the magnetization saturation is reached within 8 min and 50% within 1.5 min, illustrating the relatively fast response of the sample to light irradiation. The jump at $t = 97 \text{ min}$ observed when the laser is switched off (Figure 7a) is due to the thermalization of the sample (to 10 K) that was heated up during the irradiation process. If we assume that the process takes place in the paramagnetic regime, the temperature during the irradiation process should be around 20 K. Figure 7b depicts the variation of the reduced magnetization with the laser power. It shows that at a laser power of 150 mW/cm^2 the magnetization of the sample is

multiplied by around 2.5 due to an increase of the magnetic moments of the individual objects upon transformation of the diamagnetic $\text{Co}^{\text{III}}\text{Fe}^{\text{II}}$ pairs to magnetic $\text{Co}^{\text{II}}\text{Fe}^{\text{III}}$.

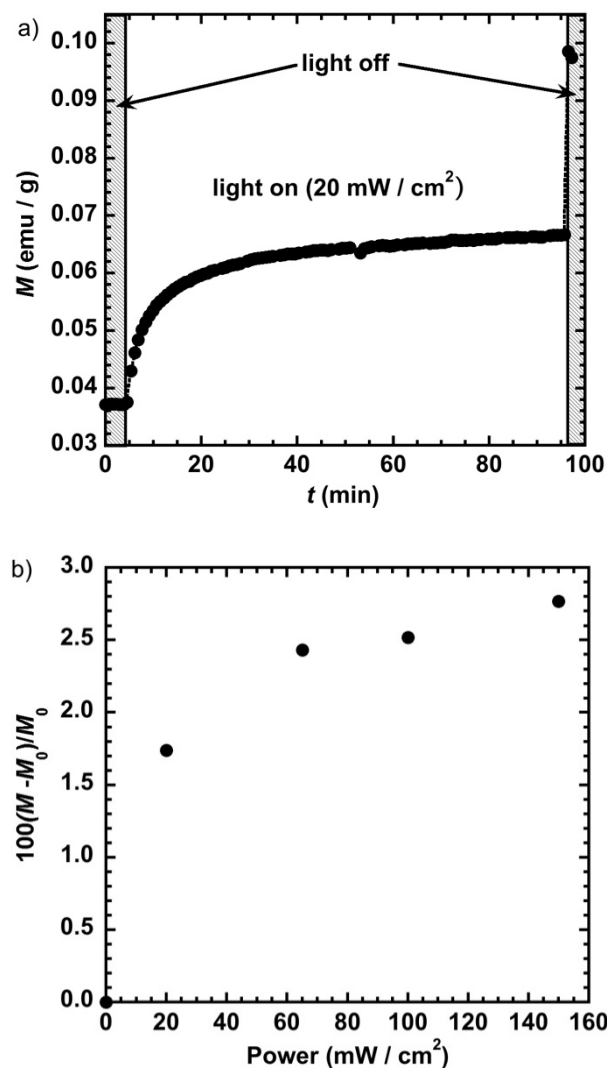


Figure 7. (a) Variation of the magnetization (M) with time (t) for a laser power of 20 mW/cm^2 and (b) reduced magnetization ($(M - M_0)/M_0$) performed at $T = 10 \text{ K}$ and $B = 0.5 \text{ T}$ showing the rate of increase of the magnetization after irradiation as a function of the laser power.

In order to assess the increase of the nanoparticles' magnetic moments with the intensity of light on the overall magnetic behavior, we measured the ZFCM curves after irradiation at $T = 2 \text{ K}$ and $B = 0.005 \text{ T}$ for laser power values of 20 , 65 , and 150 mW/cm^2 (Figure 8). The value of the maximum of the ZFCM curves shifts from 4.0 to 5.1 K when going from 20 to 150 mW/cm^2 . This behavior shows that, everything else being equal, the increase of the critical temperature is directly related to the increase of the local magnetic moments within the sample. This behavior can be due either to interparticle magnetic dipolar interactions that increase upon an increase of the objects' magnetic moments, or to an increase of the blocking temperature of the isolated objects if they were in the superparamagnetic regime. The reversibility of the process was examined by measuring the FCM curves after relaxation (heating up to $T = 250 \text{ K}$) for the different laser power values. They were all found identical to those before irradiation, showing that no damage occurs during the irradiation process even at a power of 150 mW/cm^2 .

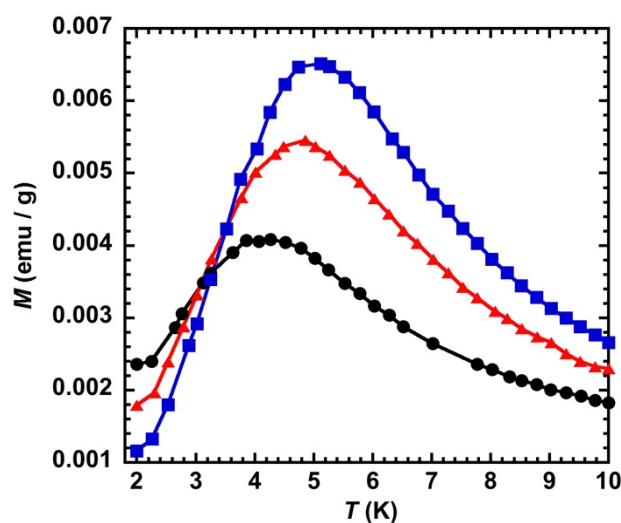


Figure 8. ZFCM after irradiation with laser power values of 20 (●), 65 (▲), and 150 (■) mW/cm², for CsCoFe_PVP.

A spin glass-like behavior was reported by us for the 3 nm Ni^{II}Fe^{III} cyanide-bridged nanoparticles [16,17]. It was also observed for CsCoFe nanoparticles, but was assigned to a size effect [18] and, later, CoFe particles embedded in mesoporous silica were investigated with the conclusion that interparticle dipolar interactions are present [19,20]. However, because of the nature of the materials (nanoparticles embedded in silica), it was not possible to investigate the effect of dilution in order to confirm that the magnetic behavior is indeed due to dipolar magnetic interactions and not to the intrinsic behavior of isolated particles. Indeed, if the particles have a size larger than that of the critical magnetic single domain size, they will have a behavior similar to that of superparamagnetic particles (single magnetic domain) feeling magnetic dipolar interactions. Moreover, it is usually difficult to reach a definite conclusion without highly diluting the nanoobjects.

We have already investigated the magnetic properties of highly diluted CsNiCr PBA particles where we demonstrated that successive dilution in PVP allows isolating the objects and observing the single domain regime with a Néel–Brown behavior and a critical size (D) of 22 nm [14]. It is possible to use this result to estimate the critical size for the CsCoFe network by comparing the magnitude of the exchange coupling interaction and the magnetic moments of the two networks. For cubic particles, D is given by $7.2(A/0.5\mu_0M^2)^{1/2}$, where A is proportional to the exchange coupling between two ions of the network and M is the magnetic moment of a pair of interacting metal ions [21]. Actually, the Co^{II}-Fe^{III} exchange coupling interaction for the CsCo^{II}Fe^{III} network is about four times weaker ($|J_{CoFe}| \approx 3.7 \text{ cm}^{-1}$) than that of CsNiCr ($J_{NiCr} \approx 16 \text{ cm}^{-1}$) [22] since its T_C is equal to 21 K [1] while that of CsNiCr is 90 K [1,22,23]. The magnetic moment of a Co^{II}Fe^{III} pair is equal to 2 Bohr Magnetons due to the antiferromagnetic coupling between $S_{Co^{II}}$ (3/2) and $S_{Fe^{III}}$ (1/2), while this value is 5 Bohr Magnetons for the CsNiCr network due to the ferromagnetic exchange coupling between Ni^{II} ($S_{Ni^{II}} = 1$ and Cr^{III} ($S_{Cr^{III}} = 3/2$). Using these values and the expression of the critical size of a single magnetic domain leads to $D = 27.5 \text{ nm}$ for the CsCoFe network, a value much larger than the size of the nanocrystals at hand (a maximum of 11 nm if light fully converts the particles from the ground diamagnetic to the metastable magnetic state), ensuring that the investigated objects are in the superparamagnetic regime. In the superparamagnetic regime, a blocking of the magnetization of the isolated objects may be observed if the magnetic correlation length is large enough for a single object to behave as single giant spin. This cannot be the case for the present nanoparticles since the Co^{II}-Fe^{III} exchange coupling interaction value ($\approx 3.7 \text{ cm}^{-1}$) is very close to the temperature maxima of the ZFCM curves (Figure 8). Consequently, the shift up of these temperature maxima upon increasing the laser power can only be due to interparticle dipolar magnetic interactions.

3. Concluding Remarks

The collective magnetic behavior of CsCoFe photoswitchable 11 nm cyanide-bridged nanoparticles was investigated by examining the effect of their dilution in two different matrices with a concentration ratio around 20 between the two compounds. The magnetic data performed in static magnetic field (FCM, ZFCM) and the susceptibility data in the presence of an alternating field are consistent with a spin glass-like behavior, compatible with interparticle magnetic dipolar interactions thanks to the analysis of the out-of-phase susceptibility data of the more concentrated sample (in CTA). For the less concentrated sample (in PVP), increasing the light intensity shifts up the temperature maximum of the ZFCM curves. The analysis of the critical single magnetic domain size and the magnetic correlation length within the objects is consistent with an interparticle dipolar coupling rather than an increase of the blocking temperature of single domain objects.

Author Contributions: Conceptualization, L.C. and T.M.; Preparation and Characterization, L.T., S.M. and E.R.; data curation, T.M.; writing—review and editing, L.C. and T.M. All authors have read and agreed to the published version of the manuscript.

Funding: This research was partially funded by the Vietnamese government for Scholarship to L.T., thesis code MN31.

Institutional Review Board Statement: Not applicable.

Informed Consent Statement: Not applicable.

Data Availability Statement: Data supporting reported results are available from the authors on request.

Conflicts of Interest: The authors declare no conflict of interest.

References

1. Sato, O.; Iyoda, T.; Fujishima, A.; Hashimoto, K. Photoinduced magnetization of a cobalt-iron cyanide. *Science* **1996**, *272*, 704–705. [[CrossRef](#)]
2. Sato, O.; Einaga, Y.; Iyoda, T.; Fujishima, A.; Hashimoto, K. Cation-driven electron transfer involving a spin transition at room temperature in a cobalt iron cyanide thin film. *J. Phys. Chem. B* **1997**, *101*, 3903–3905. [[CrossRef](#)]
3. Yokoyama, T.; Ohta, T.; Sato, O.; Hashimoto, K. Characterization of magnetic CoFe cyanides by x-ray-absorption fine-structure spectroscopy. *Phys. Rev. B* **1998**, *58*, 8257–8266. [[CrossRef](#)]
4. Sato, O.; Einaga, Y.; Fujishima, A.; Hashimoto, K. Photoinduced long-range magnetic ordering of a cobalt-iron cyanide. *Inorg. Chem.* **1999**, *38*, 4405–4412. [[CrossRef](#)]
5. Champion, G.; Escax, V.; Moulin, C.C.D.; Bleuzen, A.; Villain, F.O.; Baudalet, F.; Dartyge, E.; Verdager, N. Photoinduced ferrimagnetic systems in prussian blue analogues (C_xCo₄)-Co-I[Fe(CN)₆](y) (C-I = alkali cation). 4. Characterization of the ferrimagnetism of the photoinduced metastable state in Rb_{1.8}Co₄[Fe(CN)₆](3.3)center dot 13H₂O by K edges X-ray magnetic circular dichroism. *J. Am. Chem. Soc.* **2001**, *123*, 12544–12546. [[PubMed](#)]
6. Escax, V.; Bleuzen, A.; Moulin, C.C.D.; Villain, F.; Goujon, A.; Varret, F.; Verdager, M. Photoinduced ferrimagnetic systems in prussian blue analogues (C_xCo₄)-Co-I[Fe(CN)₆](y) (C-I = alkali cation). 3. Control of the photo- and thermally induced electron transfer by the [Fe(CN)₆] vacancies in cesium derivatives. *J. Am. Chem. Soc.* **2001**, *123*, 12536–12543. [[CrossRef](#)] [[PubMed](#)]
7. Shimamoto, N.; Ohkoshi, S.; Sato, O.; Hashimoto, K. Control of charge-transfer-induced spin transition temperature on cobalt-iron Prussian blue analogues. *Inorg. Chem.* **2002**, *41*, 678–684. [[CrossRef](#)] [[PubMed](#)]
8. Trinh, L.; Zerdane, S.; Mazerat, S.; Dia, N.; Dragoe, D.; Herrero, C.; Riviere, E.; Catala, L.; Cammarata, M.; Collet, E.; et al. Photoswitchable 11 nm CsCoFe Prussian Blue Analogue Nanocrystals with High Relaxation Temperature. *Inorg. Chem.* **2020**, *59*, 13153–13161. [[CrossRef](#)] [[PubMed](#)]
9. Brinzei, D.; Catala, L.; Louvain, N.; Rogez, G.; Stephan, O.; Gloter, A.; Mallah, T. Spontaneous stabilization and isolation of dispersible bimetallic coordination nanoparticles of Cs_xNi[Cr(CN)₆](y). *J. Mater. Chem.* **2006**, *16*, 2593–2599. [[CrossRef](#)]
10. Cammarata, M.; Zerdane, S.; Balducci, L.; Azzolina, G.; Mazerat, S.; Exertier, C.; Trabuco, M.; Levantino, M.; Alonso-Mori, R.; Glowina, J.M.; et al. Charge transfer driven by ultrafast spin transition in a CoFe Prussian blue analogue. *Nat. Chem.* **2021**, *13*, 10–14. [[CrossRef](#)]
11. Bonnet, R.; Lenfant, S.; Mazerat, S.; Mallah, T.; Vuillaume, D. Long-range electron transport in Prussian blue analog nanocrystals. *Nanoscale* **2020**, *12*, 20374–20385. [[CrossRef](#)] [[PubMed](#)]
12. Prado, Y.; Arrio, M.A.; Volatron, F.; Otero, E.; Moulin, C.C.D.; Saintavit, P.; Catala, L.; Mallah, T. Magnetic Anisotropy of Cyanide-Bridged Core and CoreShell Coordination Nanoparticles Probed by X-ray Magnetic Circular Dichroism. *Chem. Eur. J.* **2013**, *19*, 6685–6694. [[CrossRef](#)] [[PubMed](#)]

13. Dormann, J.L.; Spinu, L.; Tronc, E.; Jolivet, J.P.; Lucari, F.; D’Orazio, F. Effect of interparticle interactions on the dynamical properties of gamma-Fe₂O₃ nanoparticles. *J. Magn. Magn. Mater.* **1998**, *183*, L255–L260. [[CrossRef](#)]
14. Prado, Y.; Mazerat, S.; Riviere, E.; Rogez, G.; Gloter, A.; Stephan, O.; Catala, L.; Mallah, T. Magnetization Reversal in (CsNiCrIII)-Cr-II(CN)₆ Coordination Nanoparticles: Unravelling Surface Anisotropy and Dipolar Interaction Effects. *Adv. Funct. Mater.* **2014**, *24*, 5402–5411. [[CrossRef](#)]
15. Dormann, J.L.; Cherkaoui, R.; Spinu, L.; Nogues, M.; Lucari, F.; D’Orazio, F.; Fiorani, D.; Garcia, A.; Tronc, E.; Jolivet, J.P. From pure superparamagnetic regime to glass collective state of magnetic moments in gamma-Fe₂O₃ nanoparticle assemblies. *J. Magn. Magn. Mater.* **1998**, *187*, L139–L144. [[CrossRef](#)]
16. Brinzei, D.; Catala, L.; Rogez, G.; Gloter, A.; Mallah, T. Magnetic behaviour of negatively charged nickel(II) hexacyanoferrate(III) coordination nanoparticles. *Inorg. Chim. Acta* **2008**, *361*, 3931–3936. [[CrossRef](#)]
17. Folch, B.; Guari, Y.; Larionova, J.; Luna, C.; Sangregorio, C.; Innocenti, C.; Caneschi, A.; Guerin, C. Synthesis and behaviour of size controlled cyano-bridged coordination polymer nanoparticles within hybrid mesoporous silica. *New J. Chem.* **2008**, *32*, 273–282. [[CrossRef](#)]
18. Pajerowski, D.M.; Frye, F.A.; Talham, D.R.; Meisel, M.W. Size dependence of the photoinduced magnetism and long-range ordering in Prussian blue analogue nanoparticles of rubidium cobalt hexacyanoferrate. *New J. Phys.* **2007**, *9*, 222. [[CrossRef](#)]
19. Moulin, R.; Delahaye, E.; Bordage, A.; Fonda, E.; Baltaze, J.P.; Beaunier, P.; Riviere, E.; Fornasieri, G.; Bleuzen, A. Ordered Mesoporous Silica Monoliths as a Versatile Platform for the Study of Magnetic and Photomagnetic Prussian Blue Analogue Nanoparticles. *Eur. J. Inorg. Chem.* **2017**, 1303–1313. [[CrossRef](#)]
20. Fornasieri, G.; Bordage, A.; Bleuzen, A. Magnetism and Photomagnetism of Prussian Blue Analogue Nanoparticles Embedded in Porous Metal Oxide Ordered Nanostructures. *Eur. J. Inorg. Chem.* **2018**, 259–271. [[CrossRef](#)]
21. Rave, W.; Fabian, K.; Hubert, A. Magnetic states of small cubic particles with uniaxial anisotropy. *J. Magn. Magn. Mater.* **1998**, *190*, 332–348. [[CrossRef](#)]
22. Mallah, T.; Auberger, C.; Verdaguer, M.; Veillet, P. A Heptanuclear Cr₇(CN)₆ Complex with a Low-Lying S = 15/2 Ground-State. *J. Chem. Soc. Chem. Commun.* **1995**, 61–62. [[CrossRef](#)]
23. Gadet, V.; Mallah, T.; Castro, I.; Verdaguer, M.; Veillet, P. High-Tc Molecular-Based Magnets—A Ferromagnetic Bimetallic Chromium(III) Nickel(I) Cyanide with T_c = 90-K. *J. Am. Chem. Soc.* **1992**, *114*, 9213–9214. [[CrossRef](#)]